Chemical Engineering Science 246 (2021) 116876

Contents lists available at ScienceDirect

Chemical Engineering Science

journal homepage: www.elsevier.com/locate/ces

Kinetic modeling and simulation of high-temperature by-product formation from urea decomposition

C. Kuntz [1], C. Kuhn [1], H. Weickenmeier [1], S. Tischer [2], M. Börnhorst [1], O. Deutschmann *[,1,2]

Karlsruhe Institute of Technology (KIT), Kaiserstr. 12, 76128 Karlsruhe, Germany

HIGHLIGHTS

- Investigation of high-temperature urea by-products by TG, DSC and MS.
- Evaluation of kinetics for the decomposition of high-temperature urea by-products.
- Development of a reaction mechanism over the whole SCR relevant temperature range.
- Simulations with multiphase tank reactor model in good agreement with exp. data.

GRAPHICAL ABSTRACT

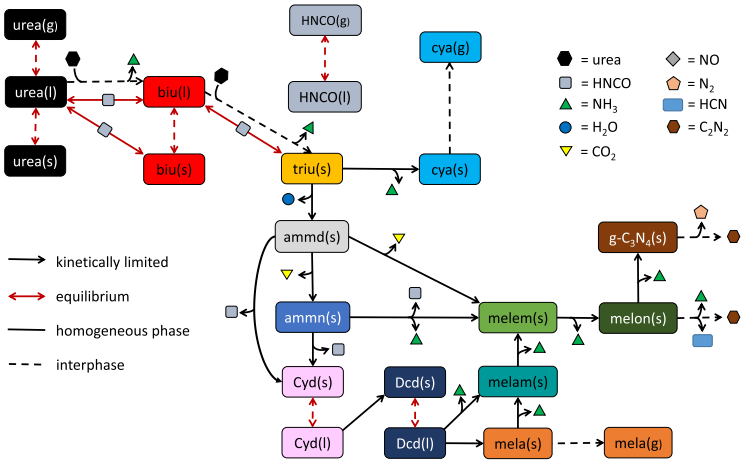

ARTICLE INFO

Article history:
Received 19 January 2021
Received in revised form 2 June 2021
Accepted 12 June 2021
Available online 17 June 2021

Keywords:
SCR
Urea decomposition
Deposit formation
Model
Kinetics

ABSTRACT

The Selective catalytic reduction (SCR) technique is widely applied in exhaust gas after-treatment of diesel engines. Depending on operating conditions, injected urea-water solution (UWS) can form liquid films on mixer blades and the pipe wall. Evaporation and subsequent reactions in the wall film can lead to deposits of urea and by-products, respectively. Especially deposits that are not decomposed up to high temperatures are challenging for the SCR technique. Thermogravimetric experiments are conducted for these stable urea by-products, such as ammelide, ammeline and their by-products, such as cyanamide or melamine. An analysis of the evolving gases during thermal decomposition led to a more detailed understanding of the kinetics. The postulated mechanism is able to predict the thermogravimetric analyses results and the effects of variation of the experimental conditions such as initial sample mass and heating rates. The evaluated kinetics, together with the recently developed kinetics for the urea/biuret/triuret/cyanuric acid system Tischer et al. (2019), can now be integrated into CFD simulations of SCR systems to numerically simulate all relevant physical and chemical processes in UWS equipped aftertreatment systems for a wide range of conditions.

1. Introduction

The control of emissions of nitrogen oxides (NO_x) is a challenge in every combustion using air as oxidizer. The need for efficient and reliable aftertreatment of NO_x emissions became obvious to

* Corresponding author.
E-mail address: deutschmann@kit.edu (O. Deutschmann).
[1] Institute for Chemical Technology and Polymer Chemistry, Karlsruhe Institute of Technology (KIT), Germany.
[2] Institute for Catalysis Research and Technology, Karlsruhe Institute of Technology (KIT), Germany.

https://doi.org/10.1016/j.ces.2021.116876
0009-2509/

Nomenclature

β_k	Temperature exponent
$\Delta_f H^{\ominus}$	Standard enthalpy of formation at 298.15 K (J mol^{-1})
$\dot{n}_{ik}$	Molar rate of species i from reaction k (mol s^{-1})
A_k	Pre-exponential factor (SI-units)
a_{ni}	Coefficient of NASA polynomials
$c_{p,i}$	Molar heat capacity of species i (J mol^{-1}K^{-1})
$E_{A,k}$	Activation energy (J mol^{-1})
H	Enthalpy (J)
$H_{m,i}$	Partial molar enthalpy of species i
k_w	Heat transfer coefficient (W m^{-2}K^{-1})
$n_{i,k}$	Reaction order
n_i	Molar amount of species i (mol)
P^{DSC}	DSC Signal (W)
R_k	Reaction number k
$S^{\ominus}$	Standard entropy at 298.15 K (J mol^{-1}K^{-1})
$S_{m,i}$	Partial molar entropy of species i (J mol^{-1}K^{-1})
T	Temperature (K or °C)
T^{ext}	Temperature of the external temperature profile (K or °C)
R	Gas constant (8.31446J mol^{-1}K^{-1})

the broad public in the last years concerning diesel fueled internal combustion (IC) engines and this need will remain in the future, in particular for the increasing number of IC engines fueled with natural gas and (green) hydrogen. Selective catalytic reduction (SCR) catalysts use ammonia to reduce the NO_x emission from IC engines. Today, this ammonia is most commonly supplied in form of a 32.5wt.% urea-water solution (UWS), which is sprayed into the hot exhaust pipe. Thermolysis and hydrolysis yield the necessary reducing agent NH_3 and CO_2. However, incomplete evaporation and decomposition of UWS droplets lead to spray-wall interaction and film formation, depending on the boundary conditions (Birkhold, 2007; Börnhorst et al., 2016; Brack et al., 2016; Lundström et al., 2011; Postrioti et al., 2015; Quissek et al., 2019). Over time, condensed urea and by-product deposits can be formed from the UWS film, which reduce the ammonia uniformity and bear the risk of increased pressure drop, up to a complete blockage of the exhaust pipe (Schaber et al., 2004; Lundström et al., 2009; Bernhard et al., 2012; Ebrahimian et al., 2012; Brack et al., 2014). Although the amount of formed high-temperature by-products of the initial injected urea mass is rather small, it is especially very important to understand their formation and decomposition, since these will only decompose at temperatures above 400 °C, which is only rarely achieved in normal SCR systems. Alternative manual removal is expensive and should be avoided. Many authors studied the formation and decomposition of urea and its by-products, giving an insight in possible reactions and kinetics (Ostrogovich and Bacaloglu, 1965; Stradella and Argentero, 1993; Fang and DaCosta, 2003; Schaber et al., 2004; Eichelbaum et al., 2010; Ebrahimian et al., 2012; Bernhard et al., 2012; Brack et al., 2014; Börnhorst and Deutschmann, 2018; Tischer et al., 2019; Wang et al., 2019; Krum et al., 2021).

Ostrogovich and Bacaloglu (1965) published one of the first semi-detailed reaction mechanism describing the thermolysis of urea with the formation of biuret, guanidine, cyanuric acid, ammelide, ammeline, melamine and several intermediate species. They investigated the yield of these deposits over time at different temperatures and established equations to calculate the respective percentage. Several years later Schaber et al. (2004) investigated the thermal decomposition of urea in an open reaction vessel using thermogravimetric analysis (TGA), differential scanning calorimetry (DSC) coupled with mass spectrometry (MS), FT-IR spectroscopy, high performance liquid chromatography (HPLC) to analyze the originated residues and ammonium ISE (ion-selective electrode) measurements. They developed a reaction scheme which is divided in four temperature regions: Up to 190 °C urea melts and decomposes, from 190 °C to 250 °C biuret decomposes and forms cyanuric acid and ammelide, from 250 °C to 360 °C cyanuric acid sublimates and in the last range above 360 °C high-temperature deposits like ammelide and ammeline are decomposed.

First detailed kinetic models for urea decomposition were developed by Ebrahimian et al. (2012) and Brack et al. (2014). Both models are based on systematic analysis of TGA experiments and evolving gases during heat up of various urea by-products, but vary in their specific reactions implemented. Several later publications either used the one or the other as basis for further development or implementation into CFD (Börnhorst et al., 2020; Budziankou et al., 2020; Habchi et al., 2015; Sun et al., 2018).

Our recent study Tischer et al. (2019) proposes a reaction mechanism for urea decomposition, that accounts for thermodynamic effects of deposit formation such as phase transitions. The presence of an eutectic mixture of urea and biuret was revealed to explain the experimental observations by Schaber et al. (2004) and Brack et al. (2014) of biuret decomposition starting at 193 °C and the formation of a foam like structure at around 210 °C. The new approach does not depend on the addition of a kind of arbitrary "matrix" species (Schaber et al., 2004; Brack et al., 2014). Furthermore a second eutectic mixture with triuret was proposed but, due to a lack of data for the thermodynamic potentials of biuret and triuret, not yet integrated to the model. It is shown that cyanuric acid rather sublimates than being decomposed, as assumed before (Ostrogovich and Bacaloglu, 1965; Eichelbaum et al., 2010). Hence, the proposed reaction mechanism can explain more effects with less assumptions than the kinetics published before. A recent study by Krum et al. (2021) modified the mechanism by (Brack et al., 2014), applying it to experiments with higher heating rates. However, all those mechanism have in common, that they do not propose any detailed scheme that goes beyond the sublimation or decomposition of ammeline and melamine, that means at temperatures above 400 °C.

Actually, Liebig (1834) was the first who published possible formation and decomposition reactions of ammelide, ammeline, melamine, melam, melem and melon, in 1834, when studying urea and its derivatives as a naturally occuring product, which could be extracted from urine. In the next 160 years, molecules with C-N bonds often were of interest to many researchers, e.g., Liu and Cohen (1989) reported a theoretical study suggesting that carbon nitride structures (C_3N_4) could have a compressibility comparable to diamond. Different modifications of C_3N_4 (Liu and Cohen, 1989; Yin et al., 2003; Yin et al., 2003) were synthesised and characterized, such as graphitic carbon nitride ($g-C_3N_4$) from urea or its byproducts (Gross and Höppe, 2020; Jürgens et al., 2003; Lotsch, 2006; Miller et al., 2017; Zhu et al., 2014). Furthermore $g-C_3N_4$ was found as a metal free catalyst and optoelectronic semiconductor (Zhang et al., 2014; Zhu et al., 2014; Ruan et al., 2015).

Lotsch and Schnick (Lotsch, 2006) work on precursors for, and the formation of, carbon nitride networks (Lotsch and Schnick, 2005; Lotsch and Schnick, 2007). A mechanism describing reactions from melamine, over the formation of melam or directly, to melem, to melon and finally to g – C3N4 via the gradual deam-

monation and polymerization was proposed and validated through several analytical, cristallographic, spectrometric, thermal and calorimetric methods.

Zhu et al. (2014) published a review paper on the synthesis, properties and applications in catalysis of graphitic carbon nitride. Several synthesis routes from cyanamide, guanidine hydrochlorine, surfactants and pure urea are gathered and discussed. Furthermore they discuss the physicochemical properties of $g-C_3N_4$. A study using TGA coupled with MS revealed that $g-C_3N_4$ can withstand temperatures up to 600 °C without significant mass loss, even in oxidizing atmosphere. It is furthermore depicted that $g-C_3N_4$ rather decomposes than being oxidized with O2. The analysis of the evolving gases with MS supports this assumption by showing the formation of NH_3, CNH and C_2N_2 and no signal for oxides like CO or CO_2.

In this work we combine the published mechanisms on urea decomposition up to ammeline with a novel mechanism for the deammonation and polymerization reactions of melamine to graphitic carbon nitride. To the best of our knowledge, for the first time a detailed kinetic scheme is proposed to capture the decomposition of urea and its by-products up to temperatures of 750 °C.

2. Experiments

For kinetic and thermodynamic investigation of high-temperature urea deposits experimental data are derived from thermogravimetric analysis (TG), differential scanning calorimetry (DSC) and mass spectroscopy (MS). follow. All TG experiments follow the same procedure for each experiment. The sample is ground and 5mg to 100mg initial mass is placed in a corundum crucible. With a constant heating rate between 2 and 10K min^{-1} the samples are heated from room temperature to 750 °C. Surrounding the crucible a purge gas flow of 100mL min^{-1} of synthetic air (20.5% O_2 in N_2) flows, if not further specified.

Pure ammelid (Dr. Ehrenstorfer GmbH, 99.4%), ammeline (Sigma Aldrich, 97.9%), cyanamide (Sigma Aldrich, 99%), dicyandiamide (Sigma Aldrich, 99%), melamin (Fluka AG, 99%) and melem (Chemos GmbH & Co. KG, 98.2%) are used for the measurements.

A *Mettler DSC 30* is used to investigate the thermal behaviour of the samples during heat up. DSC, as a thermo-analytical measurement technique, can detect exothermic or endothermic heat flows in comparison to a reference, which allows to gather data on heat capacities, heat of transition, heat of reaction or heat of a phase change (sublimation, melting or vaporization). Like in the TG experiments, the samples with an initial mass of 5 to 10mg are heated from room temperature to 750 °C with an surrounding synthetic air flow. For better heat flow measurement aluminum crucibles are used for sample and reference. Equipped to the DSC is a *Netzsch QMS 403 Aëolos Quadro* mass spectrometer to analyze the evolving gases, which are produced from the sample during heat-up.

A list of all experiments conducted in this study is given in Table 1. There, the type of the experiment, crucible type, substance, intial weight and the heating ramp is given. Experiments are either conducted as TG or DSC measurements, where the DSC experiments however include TG and MS measurements as well. The substance was either placed in a cylinder-type crucible (6mm inner diameter and 12mm height) or in a plate-type crucible (15mm inner diameter and 5mm height) in the specified setup. For each species several experiments, differing in initial mass or heating rate, are conducted to investigate the decomposition under different conditions.

3. Numerical Model

The TG and DSC experiments are simulated by our zero-dimensional batch-type reactor model (Tischer et al., 2019), which is implemented as DETCHEM^{MPTR} (MPTR: multi-phase tank reactor) in the DETCHEM software package (Deutschmann et al., 2018). Each species S_i is grouped into a specific phase P_j. Mixtures of species within a phase are considered ideal. However, by using multiple phases for liquid, aqueous and the different solid species, this assumption can be justified. A phase change of a substance is handeled by two different species in two different phases. Thermodynamic data, namely specific heat, enthalpy and entropy, for each species are calculated based on assigned NASA-polynomials (Eqs. (1)–(3)).

$$\frac{c_{p,i}}{R} = a_{1i} + a_{2i}T + a_{3i}T^2 + a_{4i}T^3 + a_{5i}T^4 \tag{1}$$

$$\frac{H_{m,i}}{R} = a_{1i}T + \frac{a_{2i}}{2}T^2 + \frac{a_{3i}}{3}T^3 + \frac{a_{4i}}{4}T^4 + \frac{a_{5i}}{5}T^5 + a_{6i} \tag{2}$$

$$\frac{S_{m,i}}{R} = a_{1i}\ln T + a_{2i}T + \frac{a_{3i}}{2}T^2 + \frac{a_{4i}}{3}T^3 + \frac{a_{5i}}{4}T^4 + a_{7i} \tag{3}$$

Species conservation (Eq. 4) and enthalpy conservation (Eq. 5) are considered by the batch reactor model. Furthermore the temperature of the system is linked to its total enthaply (Eq. 6).

$$\frac{dn_i}{dt} = \sum_{R_k} \dot{n}_{ik} \tag{4}$$

$$\frac{dH}{dt} = Ak_w\left(T^{\text{ext}} - T\right) \tag{5}$$

$$H = \sum_{S_i} n_i \cdot H_{m,i}(T) \tag{6}$$

k_w is the heat transfer coefficient of the system to its ambience, but since the experiments are driven by an external temperature profile with temperature T^{ext}, the value of k_w is not very sensitive for the simulation. Therefore, for all simulations in this work a value of

Table 1
List of conducted experiments.

Type	Crucible	Substance	Initial weight (mg)	Ramp ($Kmin^{-1}$)
TG	Cylinder	Ammelide	20.5	2
TG	Cylinder	Ammelide	9.34	10
DSC	Cylinder	Ammelide	4.6	2
TG	Cylinder	Ammeline	20.2	2
TG	Cylinder	Ammeline	30.2	2
TG	Cylinder	Ammeline	15	10
TG	Cylinder	Cyanamide	20.1	2
TG	Cylinder	Cyanamide	19.6	10
TG	Cylinder	Dicyandiamide	20.3	2
DSC	Cylinder	Dicyandiamide	7.5	2
TG	Cylinder	Melamin	25.9	2
TG	Cylinder	Melem	7.5	2

k_w = 200 W m^{-2}K^{-1} is chosen. DSC signals is the (negative) enthalpy change of all condensed species in the system. Since gas phase reactions shall not be considered in this study, the DSC signal equals the change of the total enthalpy minus the power to heat the gas (Eq. 7).

$$P^{DSC} = -\frac{dH}{dt} + \left(\sum_i^{S^{gas}} n_i c_{p,i}\right)\frac{dT}{dt} \tag{7}$$

For more information about the reactor model and calculation of the reaction rates we refer to our previous paper Tischer et al. (2019).

4. Thermodynamics and reaction mechanism

From our former study Tischer et al. (2019), we know, that thermodynamics, in particular phase transitions and eutectica, play a significant role in decomposition of urea and its by-products. With the availability of DSC measurements, the phase change, sublimation and reaction enthalphies can be considered and integrated into the thermodynamic properties of all species involved. The thermodynamic data for fundamental gaseous species, namely water H_2O(g), ammonia NH_3(g) and isocyanic acid HNCO(g), as well as their liquid or aqueous phases are taken from thermodynamic databases Tischer et al., 2019; Burcat, 2006.

In the following, the considerations, calculations and assumptions for thermodynamic properties of involved high-temperature urea by-products are discussed, a summary is given in Table 2. NASA coefficients for these species were estimated for a temperature range from 273K to 1023K (see thermdata in the supplemental information).

The proposed reaction mechanism is based on the given literature data and the experimental findings in this work, a summary of all involved reactions can be found in Table 3.

4.1. Ammelide and Ammeline

Ammelide and Ammeline (the chemical structure is given in the Supplemental Information Fig. A1) are both well known species from existing decompositon mechanisms of urea and its by-products. Their decomposition was often described as simple sublimation process (Brack et al., 2014) or as a 1-step decomposition reaction (Ebrahimian et al., 2012). Schaber et al. (2004) described the reaction from ammelide to ammeline as ammonation, however these reactions only occur at elevated pressures, which is rarely the case in SCR applications. The reaction of ammelide to ammeline is given by Eq. 8 as used in this work (Tischer et al., 2019). Furthermore a direct reaction to melem (Eq. 9) is implemented. Both reactions are clearly global reactions, but can describe the experimental findings sufficiently well.

$$3\text{ammd(s)} \rightarrow 2\text{ammn(s)} + \text{Cyd(s)} + 2CO_2 \quad \Delta_R H(300^\circ\text{C}) = -140.8\text{kJ mol}^{-1} \tag{8}$$

$$3\text{ammd(s)} \rightarrow \text{melem(s)} + \text{Cyd(s)} + 2CO_2 + 2H_2O \quad \Delta_R H(300^\circ\text{C}) = 100.5\text{kJ mol}^{-1} \tag{9}$$

Only few literature mechanisms include ammeline decomposition. Schaber et al. (2004) stated an ammonation reaction of ammeline to melamine, which however is unlikely to happen solely, due to low ammonia concentrations. A simultaneous decomposition and polymerization of ammeline with increasing temperature is more likely. A decomposition reaction of ammeline to HNCO and Cyd is proposed (Eq. 10). Furthermore an equally occuring polymerization to melam (Eq. 11) and melem (Eq. 12) is assumed.

$$\text{ammn(s)} \rightarrow \text{HNCO} + 2\text{Cyd(s)} \qquad \Delta_R H(300^\circ\text{C}) = 237.0\text{kJ mol}^{-1} \tag{10}$$

$$3\text{ammn(s)} \rightarrow \text{melam(s)} + 3\text{HNCO} \qquad \Delta_R H(300^\circ\text{C}) = 174.5\text{kJ mol}^{-1} \tag{11}$$

$$3\text{ammn(s)} \rightarrow \text{melem(s)} + 3\text{HNCO} + 3NH_3 \quad \Delta_R H(300^\circ\text{C}) = 139.4\text{kJ mol}^{-1} \tag{12}$$

4.2. Cyanamide and Dicyandiamide

Cyanamide (Cyd) is a rather simple molecule consisting of only a primary amino- and a nitrile group, which are directly connected

Table 2
Thermodynamic properties of high-temperature urea deposits in different phases (g = gas, l = liquid, s = solid). Estimations (est.) for properties not available in literature are explained in Section 4.

Species	Symbol(phase)	$\Delta_f H^\ominus$ [kJ mol^{-1}]	$S^\ominus$ [J mol^{-1}K^{-1}]	c_p [J mol^{-1}K^{-1}]	Ref.
Ammelide	ammd(s)	−492.900	149.1	$94.958 + 0.262T - 8.444 * 10^{-5}T^2 - 2.639 * 10^{6}T^{-2}$	(Tischer et al., 2019)
Ammeline	ammn(s)	−300.000	149.1	$94.958 + 0.262T - 8.444 * 10^{-5}T^2 - 2.639 * 10^{6}T^{-2}$	(Tischer et al., 2019)
Cyanamide	cyd(s)	61.300	14.7	$2.237 + 2.405 * 10^{-2}T$	(Güthner and Mertschenk, 2000)
	cyd(l)	68.300	40.8	$8.368 + 8.773 * 10^{-3}T$	(Güthner and Mertschenk, 2000), est.
Dicyandiamide	dcd(s)	21.300	127.0	$2.804 + 3.976 * 10^{-2}T$	(Güthner and Mertschenk, 2000; Zhang et al., 1997; Zhang et al., 2014)
	dcd(l)	32.800	146.0	$7.598 + 4.525 * 10^{-2}T$	(Zhang et al., 1997), est.
Melamin	mela(s)	−71.720	149.0	$-5.845 * 10^{2} + 4.857T - 1.009 * 10^{-2}T^2 + 7.101 * 10^{-6}T^3$	(Salley and Gray, 1948; Smolin and Rapoport, 1959)
	mela(g)	49.280	146.0	$21.104 + 3.886 * 10^{-3}T$	(Smolin and Rapoport, 1959; Gratzfeld and Olzmann, 2017), est.
Melam	melam(s)	0.018	530.0	$8.0215 + 6.545 * 10^{-2}T$	est.
Melem	melem(s)	15.600	530.0	$8.0215 + 6.545 * 10^{-2}T$	(Selivanov et al., 1973), est.
Melon	melon(s)	60.000	126.7	$32.94 - 0.2681T + 1.198 * 10^{-3}T^2 - 1.575 * 10^{-6}T^3 + 6.772 * 10^{-10}T^4$	(Selivanov et al., 1973), est.
Graphitic Carbon Nitride	g-C3N4(s)	412.17	126.77	$32.94 - 0.2681T + 1.198 * 10^{-3}T^2 - 1.575 * 10^{-6}T^3 + 6.772 * 10^{-10}T^4$	(Ruan et al., 2015)

Table 3
Kinetic parameters of the proposed reaction scheme. Reactions and kinetics for the low-temperature range up to 400 °C, indicated by a ∗, are taken from Tischer et al. (2019).

Reaction	$n_{i,k}$	A_k	β_k	$E_{A,k}$ /kJ mol^{-1}
Homogeneous phase				
ammd(s) → 2HNCO + 2Cyd(s)	1	$4.0 \cdot 10^{10}$	0	175.67
3ammd(s) → 2ammn(s) + Cyd(s) + 2CO_2	3	$1.0 \cdot 10^{15}$	0	185.67
3ammd(s) → melem(s) + Cyd(s) + 2CO_2 + 2H_2O	1	$1.5 \cdot 10^{14}$	0	185.67
ammn(s) → HNCO + 2Cyd(s)	1	$8.0 \cdot 10^{10}$	0	187.67
3ammn(s) → melem(s) + 3HNCO + 2NH_3	1	$1.0 \cdot 10^{11}$	0	200.67
3ammn(s) → melam(s) + 3HNCO + NH_3	1	$1.0 \cdot 10^{11}$	0	200.67
2Cyd(l) → Dcd(s)	2	$9.0 \cdot 10^{8}$	0	115.67
3Dcd(l) → 2mela(s)	1	$2.0 \cdot 10^{12}$	0	165.67
3Dcd(l) → melam(s) + NH_3	1	$4.0 \cdot 10^{12}$	0	165.67
3Dcd(l) → 6HCN + 2NH_3 + 2N_2	1	$1.7 \cdot 10^{12}$	0	165.67
2mela(s) → melam(s) + NH_3	1	$2.0 \cdot 10^{9}$	0	157.67
melam(s) → melem(s) + NH_3	1	$3.0 \cdot 10^{12}$	0	215.67
melam(s) → 6HCN + NH_3 + 2N_2	1	$0.6 \cdot 10^{12}$	0	215.67
melem(s) → melon(s) + NH_3	1	$2.5 \cdot 10^{3}$	0	130.71
melem(s) → 2g − C_3N_4(s) + 2NH_3	1	$1.2 \cdot 10^{3}$	0	130.71
∗ urea(l) + HNCO(l)⇌biu(s)	1 + 1	$1.0 \cdot 10^{-4}$	0	0
∗ urea(l) + HNCO(l)⇌biu(l)	1 + 1	$1.0 \cdot 10^{-4}$	0	0
∗ biu(l) + HNCO(l)⇌triu(s)	1 + 1	$1.0 \cdot 10^{-4}$	0	0
∗ triu(s) → cya(s) + NH_3	1	$1.2 \cdot 10^{2}$	0	45
∗ triu(s) → ammd(s) + H_2O	1	$3.0 \cdot 10^{1}$	0	45
Surface				
mela(s) → mela(g)	1	$9.0 \cdot 10^{5}$	0	141.3
melon(s) → 2g − C_3N_4(s) + NH_3	1	$7.5 \cdot 10^{0}$	0	149.7
5melon(s) → 9C_2N_2 + 12HCN + NH_3 + 7N_2	1	$3.0 \cdot 10^{1}$	0	149.7
2g − C3N4(s) → 3C_2N_2 + N_2	1	$2.8 \cdot 10^{1}$	0	149.7
∗ 2urea(l) → biu(l) + NH_3	2	$3.5 \cdot 10^{0}$	0	99.0
∗ biu(l) + urea(l) → triu(s) + NH_3	1 + 1	$2.0 \cdot 10^{2}$	0	116.5
∗ cya(s) → cya(g)	1	$30.0 \cdot 10^{4}$	0	141.3
Phase change				
Cyd(s)⇌Cyd(l)	1	$8.8 \cdot 10^{-2}$	0	0
Dcd(s)⇌Dcd(l)	1	$8.8 \cdot 10^{-2}$	0	0
∗ H_2O(g)⇌H_2O(l)	1	$8.6 \cdot 10^{-2}$	0.5	0
∗ urea(g)⇌urea(l)	1	$4.7 \cdot 10^{-2}$	0.5	0
∗ HNCO(g)⇌HNCO(l)	1	$5.5 \cdot 10^{-2}$	0.5	0
∗ urea(l)⇌urea(s)	1	$1.0 \cdot 10^{-6}$	0	0
∗ biu(l)⇌biu(s)	1	$1.0 \cdot 10^{-6}$	0	0

to each other. Thus, it has two reactive centres, one *nucleophilic* and one *electrophilic* (Michaud et al., 1988). Therefore, Cyanamide is a very reactive molecule. Due to the two functional groups it is able to cyclize or polymerise. During heat up Cyd starts to melt at 46 °C with a latent heat of fusion of 8.76kJ mol^{-1} (Güthner and Mertschenk, 2000). Unless kept cool or stabilized, the dimerization of Cyd can occur rather violently, but starts noticeably at about 150 °C (Eq. 14). The enthalpy of dimerization to dicyandiamide at 25 °C is -48.8kJ mol^{-1} (Güthner and Mertschenk, 2000). Further decomposition of Cyd is discussed in the following as it overlaps with its dimerization product.

$$\text{Cyd(s)}\rightleftharpoons\text{Cyd(l)} \qquad \Delta_R H(47^\circ\text{C}) = 8.76\text{kJ mol}^{-1} \tag{13}$$

$$\text{2Cyd(l)} \rightarrow \text{Dcd(s)} \qquad \Delta_R H(47^\circ\text{C}) = -59.8\text{kJ mol}^{-1} \tag{14}$$

Dicyandiamide (Dcd) is the dimer of cyanamide, also known as cyanoguanidine. It is an odorless, colorless, nonvolatile powder with a monoclinic primatic crystal structure (Hirshfeld and Hope, 1980; Güthner and Mertschenk, 2000). Güthner and Mertschenk (2000) reported an enthalpy of formation of 18.4kJ mol^{-1} at 25 °C, a thermal stability of up to 170 °C and a melting point of 210-212 °C, which depends on the heating rate. The melting starts at 208.44 °C with a peak at 214.41 °C as reported by Zhang et al. (1997), which fits well into the previous range. Furthermore, a molar enthalphy and entropy of melting was determined by DSC as 22.96kJ mol^{-1} and 47.68J K^{-1} mol^{-1}, respectively (Zhang et al., 1997). The specific heat, obtained by DSC, is given in 5K-steps from 305K to 465K as 122.49-171.02J K^{-1} mol^{-1}, which can be approximated up to its melting point by a linear regression function as given in Table 2. The specific heat of 264.57J K^{-1} mol^{-1} at 495K can be interpreted as the liquid phase ones. Calculated Gibbs free energies for Cyd and Dcd, both for solid and liquid phase, are shown in Fig. 1. Melting points, marked by the temperature where curves for solid and liquid phase intercept, are highlighted with black circles and given as previously discussed. TG curves of Cyd and Dcd at different heating rates and initial masses, as well as a DSC curve for Dcd, are given in Fig. 2.

As can be denoted from the TG curves the decomposition of Cyd and Dcd is overlapping and it can be clearly seen, that Cyd dimerizes to Dcd (Eq. 14). Furthermore, melting of Dcd (Eq. 15) can be observed at about 211 °C, which is also in good agreement with literature data (Zhang et al., 1997; Güthner and Mertschenk, 2000; Zhang et al., 2014). As soon as Dcd melts, first decomposition starts. As shown in Bojdys (2009), Dcd can react either to melamine (Eq. 16) or directly to melam (Eq. 17). In addition, small parts are directly decomposed to gaseous HCN, NH_3 and nitrogen (Eq. 18).

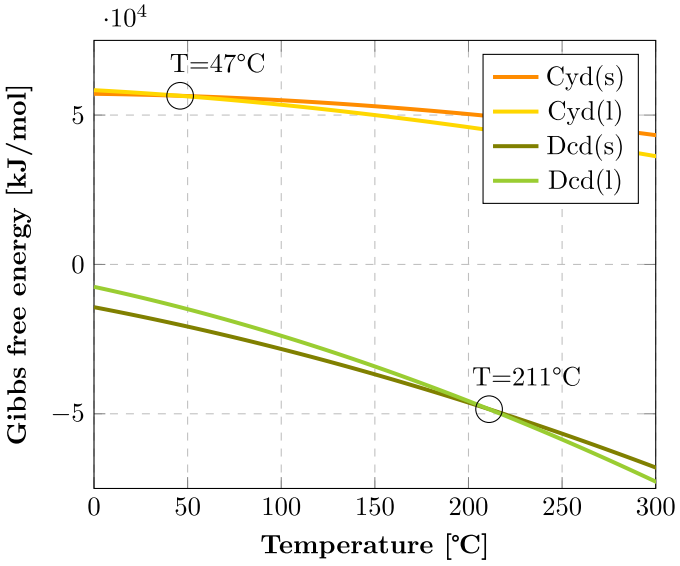

Fig. 1. Gibbs free energy of cyanamide and dicyandiamide in liquid and solid phase.

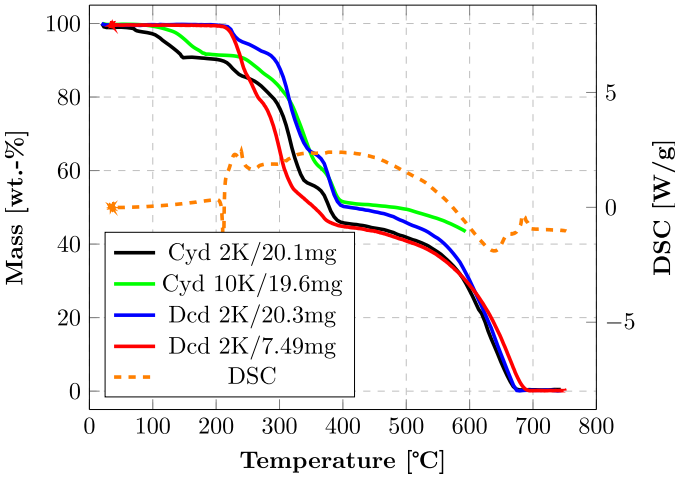

Fig. 2. Experimental TG data for decomposition of cyanamide (Cyd) and dicyandiamide (Dcd) at different heating rates and initial masses. DSC signal for DCD experiment "2 K/ 7.49 mg".

$$\mathrm{Dcd(s)} \rightleftharpoons \mathrm{Dcd(l)} \qquad \Delta_R H(211^\circ\mathrm{C}) = 25.0\,\mathrm{kJ\ mol^{-1}} \tag{15}$$

$$3\,\mathrm{Dcd(l)} \rightarrow 2\,\mathrm{mela(s)} \qquad \Delta_R H(211^\circ\mathrm{C}) = -96.7\,\mathrm{kJ\ mol^{-1}} \tag{16}$$

$$3\,\mathrm{Dcd(l)} \rightarrow \mathrm{melam(s)} + \mathrm{NH_3} \qquad \Delta_R H(211^\circ\mathrm{C}) = -68.2\,\mathrm{kJ\ mol^{-1}} \tag{17}$$

$$3\,\mathrm{Dcd(l)} \rightarrow 6\,\mathrm{HCN(g)} + 2\,\mathrm{NH_3(g)} + 2\,\mathrm{N_2} \qquad \Delta_R H(211^\circ\mathrm{C}) = 179.2\,\mathrm{kJ\ mol^{-1}} \tag{18}$$

4.3. Deammonation process to graphitic carbon nitride

Since the work of Liu and Cohen (1989) proposed carbon nitrides as super-hard materials, many researchers were emphasized to work on synthesis routes to form them from C/N/H-species. But already about 150 years earlier research was done on different nitrogen molecules.

Melamine was first prepared by Liebig (1834) in 1834. During heat up, he described a melt that pulls itself up on the walls of the tube, without sublimation, but decomposition with evolving ammonia and a lemon-colored residue. Later on, several works discussed either a decomposition (Smolin and Rapoport, 1959) or a sublimation (Mccellan, 1940; Crews et al., 2000). For this work both approaches are used and implemented, as described in Bann and Miller (1958) with "When heated, melamine sublimes with some decomposition". TG data of melamine for various heating rates and initial masses (Fig. 3) show that less than 5% is decomposed or polymerized and the most of it sublimates. Low heating rates and therefore more time at polymerization temperatures promote the formation of a residual and vice versa, for example for high heating rates the sublimation prevails and occurs almost exclusively. Furthermore, one can see that a high heating rate and a high initial mass shift the TG curve to higher temperatures, whereas with low heating rates and low initial masses the decomposition takes place at lower temperatures, as it is closer to an equilibrium state. (see Fig. 4).

The sublimation of melamine and its respective reaction enthalpy is denoted in Eq. 19. As polymerization product either melam (Smolin and Rapoport, 1959; Lotsch, 2006; Wirnhier et al., 2013) and/or melem (Smolin and Rapoport, 1959; Lotsch, 2006) is given in the literature. Several reports claim that they produced melam by pyrolizing melamine, which was later identified as melem by IR and UV spectroscopy. In contrast to that, May (1959) reported the formation of melam, melem and melon as pyrolysis products of melamine at 360 °C, 400 °C and 500 °C, respectively. Therefore the decomposition of melamine is described for both possible routes, to melam (Eq. 20) and to melem (Eq. 21).

$$\mathrm{mela(s)} \rightarrow \mathrm{mela(g)} \qquad \Delta_R H(340^\circ\mathrm{C}) = 121.3\,\mathrm{kJ\ mol^{-1}} \tag{19}$$

$$2\,\mathrm{mela(s)} \rightarrow \mathrm{melam(s)} + \mathrm{NH_3(g)} \qquad \Delta_R H(200^\circ\mathrm{C}) = 43.0\,\mathrm{kJ\ mol^{-1}} \tag{20}$$

$$2\,\mathrm{mela(s)} \rightarrow \mathrm{melem(s)} + 2\,\mathrm{NH_3(g)} \qquad \Delta_R H(200^\circ\mathrm{C}) = 23.4\,\mathrm{kJ\ mol^{-1}} \tag{21}$$

Thermodynamic data for solid melamine is obtained from Salley and Gray (1948) and Smolin and Rapoport (1959). Based on solid melamine's sublimation enthalpy of 121.3kJ mol^{-1} at 340 °C from Smolin and Rapoport (1959) and melamine's gas phase standard enthalpy of formation of 70.1kJ mol^{-1} from Gratzfeld and Olzmann (2017), the thermodynamic data for gaseous melamine are calculated. Due to the lack of sufficient literature data a 2nd

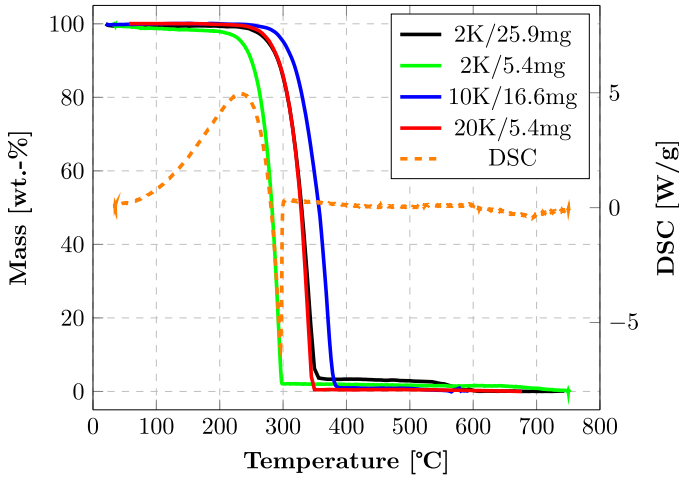

Fig. 3. Experimental TG data for decomposition of melamine at different heating rates and initial masses. DSC signal for experiment "2 K/ 5.4 mg".

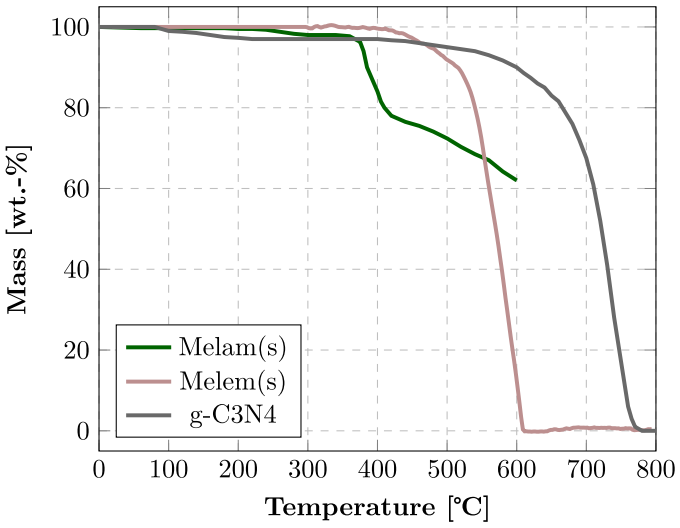

Fig. 4. Experimental TG data for decomposition of melam (data from (Wirnhier et al., 2013)), melem and graphitic carbon nitride (GCN) (data from (Zhu et al., 2014)) at different heating rates and initial masses.

order polynomial for specific heat is used. Starting from melamine, the deammonation process leads to melam, then melem, then melon and last of all to graphitic carbon nitride. During this process the H-content is successively decreasing, leaving only C-N bonds behind. Melam, as the first product of the elimination of ammonia, is formed by linking two molecules of melamine as a "ditriazinylamine"-type structure (Eq. 20). Melem can be formed either from melam by release of one ammonia (Eq. 22) or by direct deammonation of two molecules of melamin with release of two ammonia (Eq. 21). Melam and melem are structural and thermodynamically very similar, therefore they are assigned the same specific heat in this work. In general, there are only few studies on thermodynamic data for the deammonation products. Selivanov et al., 1973 reported calculated standard formation enthalpies for different products and Lotsch (2006) analyzed the crystalline structures of several C/N/H spezies, but no reliable data for specific heats can be found. For this reason the specific heat for g – C_3N_4 calculated by Ruan et al. (2015) is used for melam and melem.

$$\text{melam(s)} \rightarrow \text{melem(s)} + \text{NH}_3 \qquad \Delta_R H(300^\circ\text{C}) = -35.0\text{kJ mol}^{-1} \tag{22}$$

$$\text{melam(s)} \rightarrow 6\text{HCN} + \text{NH}_3 + 2\text{N}_2 \qquad \Delta_R H(300^\circ\text{C}) = 742.3\text{kJ mol}^{-1} \tag{23}$$

By release of another ammonia molecule during decomposition of melem, melon is formed (Eq. 24). In literature, there is no accurate structure of melon, apart from its empirical formula $C_6N_9H_3$. Structure models based on a cyameluric heptazine core C_6N_7 or triazine based models are discussed. Most appropriate is its description as a mixture of molecules of different sizes and shapes, which gives it an amorphous character (Smolin and Rapoport, 1959). To the best of our knowledge, except from a standard formation enthalpy from Selivanov et al., 1973, there is no thermodynamical data for melon in the literature. Therefore the thermodynamic data from g – C_3N_4 is used for melon, since both are very similar in their structure.

$$\text{melem(s)} \rightarrow \text{melon(s)} + \text{NH}_3 \qquad \Delta_R H(400^\circ\text{C}) = 395.1\text{kJ mol}^{-1} \tag{24}$$

$$\text{melem(s)} \rightarrow 2\text{g-C}_3\text{N}_4\text{(s)} + 2\text{NH}_3 \qquad \Delta_R H(400^\circ\text{C}) = 914.3\text{kJ mol}^{-1} \tag{25}$$

Graphitic carbon nitride is the final product of the deammonation of melamine. It consists of only C – N bonds and has a general formula of C_3N_4. Two possible structures for carbon nitrides are discussed in the literature: Triazine based graphitic carbon nitride (TGCN) and tri-s-triazine or polytriazine-imide (PTI) structures (Miller et al., 2017). TGCNs can be produced from designed unimolecular precursors and are not expected to form in large amounts from C/N/H-species, which rather form PTIs instead. As starting material for the formation of g – C_3N_4, species with C/N/H composition, like urea or its decomposition products, are favored. Miller et al. (2017) also reported, that even at high temperature not all H could be removed from the sample, but rather C_2N_2 and other volatile $C_xN_yH_z$ species evolved to the gas phase. These are the products from its pyrolysis reaction (see Eq. 28). Due to the unknown structure and reduced complexity for the simulation, the composition of graphitic carbon nitride in this work is set to C_3N_4, but decomposition is in the same temperature range as the pyrolysis of melon (see Eq. 27), to ensure the evolution of C_2N_2 and HCN at the same time. Bojdys (2009) emphasized this theory with MS measurements of g – C_3N_4 decomposition, showing the formation of C_2N_2, HCN and NH_3 in the range between 500 °C and 800 °C.

$$\text{melon(s)} \rightarrow 2\text{g-C}_3\text{N}_4\text{(s)} + \text{NH}_3 \qquad \Delta_R H(400^\circ\text{C}) = 519.2\text{kJ mol}^{-1} \tag{26}$$

$$5\text{melon(s)} \rightarrow 9\text{C}_2\text{N}_2 + 12\text{HCN} + \text{NH}_3 + 7\text{N}_2 \qquad \Delta_R H(400^\circ\text{C}) = 408.4\text{kJ mol}^{-1} \tag{27}$$

$$2\text{g-C}_3\text{N}_4\text{(s)} \rightarrow 3\text{C}_2\text{N}_2 + \text{N}_2 \qquad \Delta_R H(400^\circ\text{C}) = -88.0\text{kJ mol}^{-1} \tag{28}$$

Thermodynamic data for g – C_3N_4 are well described in the theoretical study by Ruan et al. (2015), who calculated heat capacity, enthalphy, entropy and Gibbs free energy. From this, the necessary NASA polynomial is calculated with very good agreement in the temperature range from 0 °C to 750 °C.

As a result of the investigations in this work, the authors came up with a reaction scheme of the decomposition of urea and its by-products (Fig. 5). The gathered and calculated thermodynamic data for all mentioned species is summarized in Table 2. All involved reactions for the formation and decomposition of high temperature urea by-products and their kinetic data is shown in Table 3. For each reaction the reaction order $n_{i,k}$, pre-exponential factor A_k in SI-units and the activation energy $E_{A,k}$ are given. After the kinetic data were adjusted to agree to the main characteristics of DSC and TG experimental data, no significant improvement was achieved by a following automated parameter optimization, which is why the manually fitted parameter are used in this publication.

5. Simulation results

All simulations presented in the following were performed with the DETCHEM$^{\text{MPTR}}$ software package described in Section 3 and the reaction mechanism and kinetic data from Table 3.

Starting from the decomposition of g – C_3N_4, the simulation of every species involved in the published mechanism is compared to available experimental data. In all following figures the experimental and simulated TG results are normalized by the initial mass of the experiment and plotted against the temperature.

Additional experimental and simulation results, e.g. different heating rates, and the gas composition during experiments can be found in the supplemental information section D.

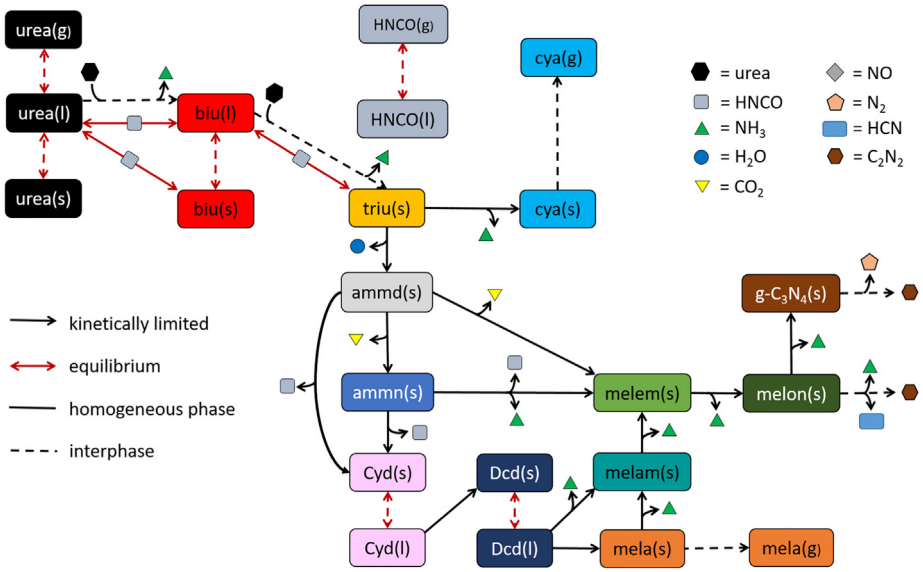

Fig. 5. Proposed reaction scheme of the decomposition of urea and its by-products. Adapted and extended from Tischer et al. (2019).

5.1. Graphitic carbon nitride

Graphitic carbon nitride is the most thermal stable solid product of the deammonation process and consists, theoretically, of only C – N bonds. Zhu et al. (2014) showed that g – C_3N_4 is not harmed by oxidizing atmosphere and pyrolizes with evolution of C_2N_2, HCN and ammonia. The occurence of H atoms in the pyrolysis gas can be attributed to an incomplete deammonation and existence of melon in the investigated sample. For the simulation pure g – C_3N_4 is used, therefore no HCN or ammonia but only C_2N_2 and nitrogen are formed. A comparison of the experiment from Zhu et al. (2010) and the simulation is shown in Fig. 6.

The initial mass reduction in the experiment is attributable to evaporating water due to humidity and is not considered in the simulation. For the following decomposition in a 1-step reaction a very good agreement between experiment and simulation is accomplished.

5.2. Melem

Since no literature data of pure melon decomposition nor the species itself for experiments is available, the next discussed species is melem. It is the third most thermal stable species in the deammonation process and melon is directly formed from melem together with g – C_3N_4 and ammonia. Melem decomposition slowly starts at around 400 °C, but takes to 500 °C for a mass loss of 10% and to 600 °C to have all melem and resulting products converted, as can be seen in Fig. 7.

The simulation of melem decomposition is in very good agreement with the experimental results. Kinetics are designed, that one third of melem reacts directly to 2 g – C_3N_4 and evolving ammonia, and two third react to melon as intermediate species. This distribution ensures a gas evolution of C_2N_2, HCN and NH_3 during the further decomposition of melon and g – C_3N_4 similiar to the experiment.

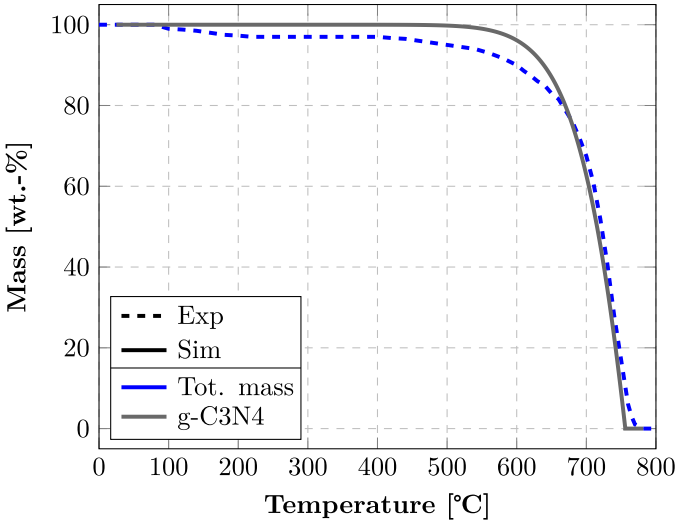

Fig. 6. Mass loss of graphitic carbon nitride as function of temperature measured by TG (cylinder crucible, 20mg, 10K min^{-1}), dashed line, and simulation results of the total mass loss of g – C_3N_4 during decomposition, solid lines. Experimental data from (Zhu et al., 2010).

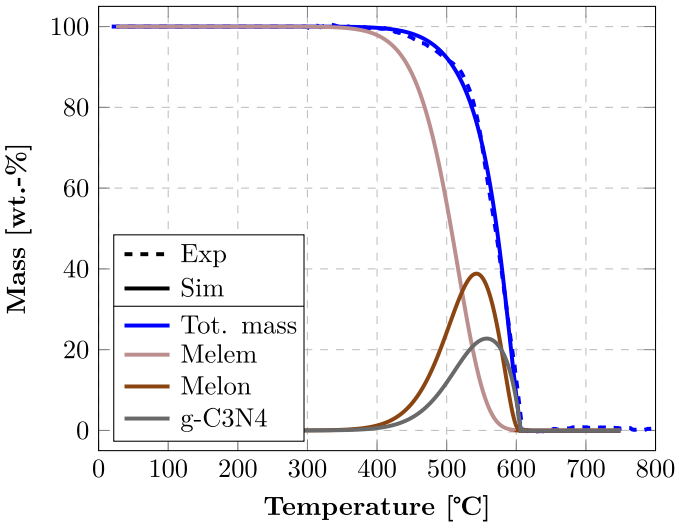

Fig. 7. Mass loss of melem as function of temperature measured by TG (cylinder crucible, 7.5mg, 2K min^{-1}), dashed line, and simulation results of the total mass loss and mixture composition during decomposition, solid lines.

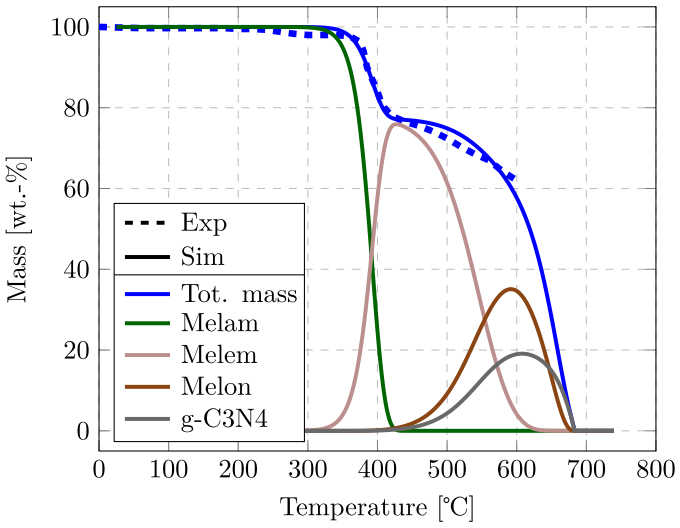

Fig. 8. Mass loss of melam as function of temperature measured by TG (cylinder crucible, 24mg, 5K min^{-1}), dashed line, and simulation results of the total mass loss and mixture composition during decomposition, solid lines. Experimental data from Wirnhier et al. (2013).

5.3. Melam

Melam is the intermediate species of the deammonation of melamin to melem and further products. It consists of two melamine rings connected by elimination of ammonia. Wirnhier et al. (2013) synthesized the rather unstable melam by thermal treatment of Dcd in an autoclave. Subsequent thermal analysis revealed the decomposition behavior, as it can be seen in Fig. 8. Melam starts to react at about 370 °C with a mass loss of 22.6% up to 410 °C. This corresponds well with evolution of either 3mol of ammonia (calc. 21.7% (Wirnhier et al., 2013)) or 1mol ammonia, 1mol HCN and 1/3mole N_2 (calc. 22.7%) per mole of melam. The latter is used in this work, which is implemented via the deammonation reaction of melam to melem (Eq. 22) and and decomposition of melam (Eq. 23).

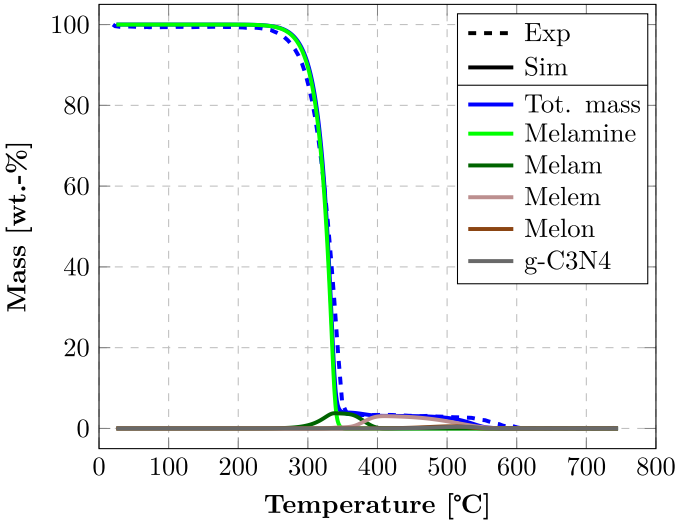

Fig. 9. Mass loss of melamine as function of temperature measured by TG (cylinder crucible, 25.9mg, 2K min^{-1}), dashed line, and simulation results of the total mass loss and mixture composition during decomposition, solid lines.

Following to melam is the decompostion of melem, where a good agreement between experiment and simulation could already be validated for the pure substance.

5.4. Melamine

A comparison between experimental data and simulation results for melamine decomposition is shown in Fig. 9. Melamine starts to react at about 250 °C. From many literature studies it is known that it mostly sublimates and only a fraction reacts to melam in open vessels. This behavior is well described in the simulation, where the mass loss of 96.25% up to 350 °C overlaps with the experiment. In the following, the produced melam reacts further to melem, melon and g – C_3N_4 and decomposes. Though, the last decomposition step of melon and g – C_3N_4 is slightly overpredicted and shifted to lower temperature. This is most probably caused by the low remaining mass and definition of the reactions on the surface, which results in high surface/volume ratios and therefore increased reactions rates.

5.5. Cyanamid

Decomposition of Cyanamide involves several stages and intermediate species. Starting from room temperature, Cyd melts at 47 °C to liquid Cyd. Simultaneously, water evaporates slowly from Cyd, even after drying, since it is a strongly hygroscopic species. Since this phenomenon could not be included in the simulation, it is always a bit above the experimental curve, which can be seen in the following. At around 100 °C liquid Cyd begins to dimerize to dicyandiamide. Interestingly, although solid Dcd is formed from the dimerization, the thermodynamic equilibrium is on the liquid Dcd side until 50% of Cyd is converted. That is caused by the liquid phase definitions and algorithm in the used model, but could occur in the experiment as well. With increasing temperature solid Dcd starts to melt at 211 °C and slowly polymerizes to melamin and decomposes in small amounts. The following mass loss due to sublimation of melamin fits very well with the experimental mass loss around 300 °C. The next stage during melam formation and decompostion to melem is in good agreement with the experiment, as can be see in Fig. 10. The last large mass loss step, starting at 400 °C, due to the formation and decomposition of melem, melon and g – C_3N_4, is again slightly overpredicted and shifted to lower temperatures, due to the mentioned problems with water and the g – C_3N_4 decomposition. Furthermore, due to the high reactivity

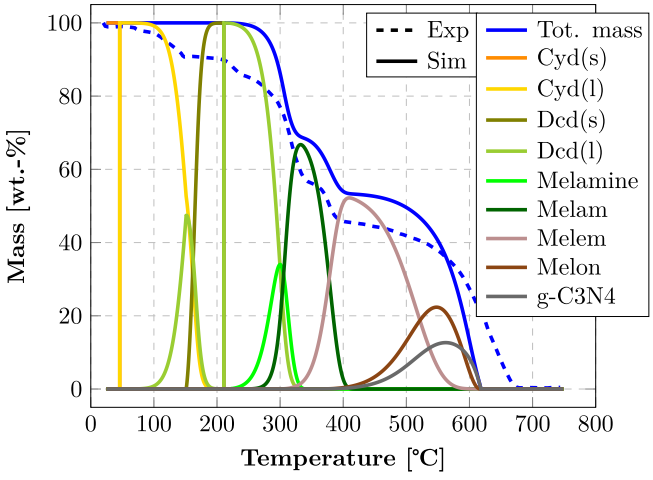

Fig. 10. Mass loss of cyanamide as function of temperature measured by TG (cylinder crucible, 20.1mg, 2K min^{-1}), dashed line, and simulation results of the total mass loss and mixture composition during decomposition, solid lines.

of Cyd with its two reactive centres it can form a diversity of side-products, which is not included in this mechanism.

The decomposition of Dcd follows the curve of Cyd in the experiment as well as in the simulation. It includes the exact same stages and formed products in the temperature ranges and is therefore not further discussed. A comparison between experiment and simulation of two measurements of Dcd decomposition, including DSC/MS data, can be found in the supplemental information.

5.6. Ammelide

Ammelide is one of the species which is already included in former reaction mechanisms. However, its decomposition was often modeled as a pure sublimation, as a simplification of the more complex real process. From the experiment in Fig. 11 it can be clearly seen, that ammelide decomposition involves more than just one reaction or stage. The simulation can reproduce this behavior with a very good agreement. Starting at about 320 °C, ammd decomposes to ammn with release of Cyd and CO_2. Simultaneously, a small part reacts directly to melem, while another part decomposes to HNCO and Cyd. Through the release of Cyd in the reactions many side products can be formed, as already discussed above. The two overlapping, but recognisable, stages in the experiment during the first decomposition of ammd could not be seperated in the simulation in that way. However, the overall mass loss of 75% up to 470 °C in the experiment is well met with the simulation (72.1%). The start of the last stage of decomposition is in good agreement, even if the mass loss with increasing temperature occurs slightly slower in the experiment than in the simulation. Residual mass in the experiment is presumably due to measurement inaccuracy. Results of the DSC/MS-measurement and a TG experiment with higher heating rate, together with corresponding simulations, can be found in the supplemental information. (see Fig. 12).

5.7. Ammeline

Ammeline decomposition starts at about 375 °C and loses 58% of its initial mass up to 475 °C. The simulation is in very good agreement (56% mass loss) with the experiment by modeling the decomposition by equal shares of melam and melem. Furthermore, ammeline pyrolizes to HNCO and Cyd as its building blocks to form other byproducts. Formed melam reacts quickly to melem by deammonation. The following decomposition stage of melem is in good agreement, but again slightly shifted to lower temperatures as already described above.

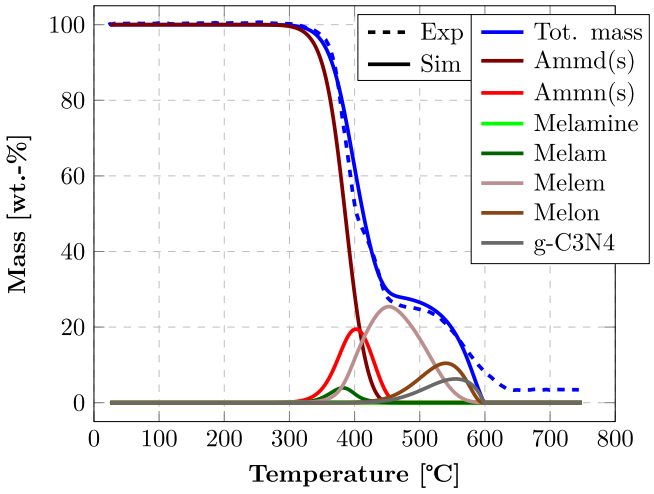

Fig. 11. Mass loss of ammelide as function of temperature measured by TG (cylinder crucible, 20.5mg, 2K min^{-1}), dashed line, and simulation results of the total mass loss and mixture composition during decomposition, solid lines.

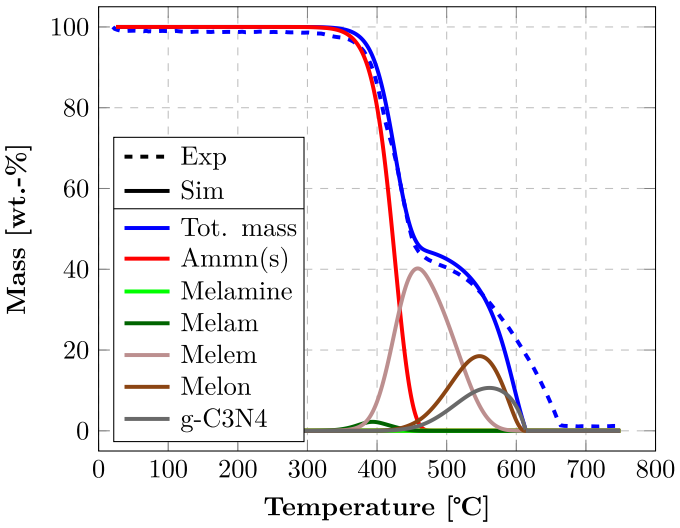

Fig. 12. Mass loss of ammeline as function of temperature measured by TG (cylinder crucible, 20.2mg, 2K min^{-1}), dashed line, and simulation results of the total mass loss and mixture composition during decomposition, solid lines.

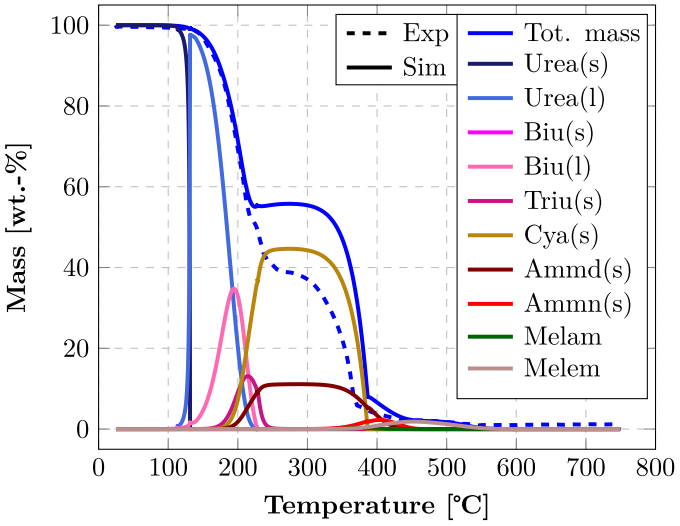

Fig. 13. Mass loss of urea as function of temperature measured by TG (cylinder crucible, 23.2mg, 2K min^{-1}), dashed line, and simulation results of the total mass loss and mixture composition during decomposition, solid lines.

5.8. Urea

The comparison between experiment and simulation for urea decomposition is shown in Fig. 13, which is the initiating species for solid deposits in SCR applications. For the simulation of urea decomposition up to ammelide formation, our recently published kinetics (Tischer et al., 2019) are used, while subsequent reactions are taken from this study. The first decomposition stage between 133 °C and 220 °C with a mass loss of 48% is well described by the model. But especially for the second decomposition stage, where biuret and triuret react, there is a significant deviation between experiment and simulation. The mechanism by Tischer et al. (2019) is not able to precisely reproduce this second stage

with a mass loss of about 13%, but forms cya and ammd earlier instead. Due to missing thermodynamic data of biuret and triuret in solid and liquid phase, no eutectic mixture of these compounds could be established as suggested (Tischer et al., 2019). The following decomposition stage involves the sublimation of cya and further decomposition of ammd. Especially above 400 °C, where all cya has sublimated, there is a good agreement between experiment and simulation. This suggests that the amount of ammd is correctly predicted by the mechanism of Tischer et al. (2019). Though, above 400 °C only 5% of the initial urea mass is left as a deposit, it is important to have a good correlation for the formation and decomposition of these high-temperature urea by-products.

6. Conclusion

This study presents a new kinetic model for high-temperature urea deposit formation and decomposition starting from ammelide. Based on TG- and DSC-measurements of the urea by-products ammelide, ammeline, cyanamide, dicyandiamid, melamin and melem and MS analysis of the evolving gases a mechanism is developed. All experiments are simulated with the DETCHEM^{MPTR} code (Tischer et al., 2019) and kinetics are manually adjusted to agree with the main characteristics of TG- and DSC data. No significant improvement of the results was achieved by a following automated parameter optimization, which is why the manually fitted parameters are used in this publication to prevent overfitting.

Other mechanisms in the literature are often limited to reactions up to the formation of ammelide or melamine and their direct decomposition into the gas phase. High-temperature by-products are not taken into account. Even if this high-temperature species make less than 5% of the initially injected urea mass, over time they can accumulate and build deposits that can only be removed by temperatures much higher than 400 °C or by expensive manual removal.

This study attemps to fill the gap of literature mechanisms by involving the formation and decomposition of 11 different species (Ammelide, Ammeline, Cyanamide solid and liquid, Dicyandiamide solid and liquid, Melamine, Melam, Melem, Melon and Graphitic Carbon Nitride), including two phase changes and the evolution of 6 different gases (CO_2, HNCO, NH_3, HCN, C2N2 and N_2). It therefore consists of 14 homogeneous and 6 interphase reactions in addition to the mechanism by Tischer et al. (2019) comprising urea reactions below 400 °C. For each species, thermodynamic data was gathered from the literature and NASA-polynomials are calculated. However, data is not available for every species and some assumptions based on similarities to other species had to be made. All performed TGA- and DSC measurements are very well described by the postulated mechanism. Even changes of initial mass or heating rate can be reproduced well. In combination with the Tischer mechanism (Tischer et al., 2019) the proposed overall reaction scheme for urea decomposition up to 750 °C gathers 21 different solid, liquid and aqueous species, 10 gaseous species, 19 homogeneous reactions, 7 interphase reactions and 7 phase change reactions.

This study presents the first reaction mechanism for decomposition of urea and formation and decomposition of its by-products over the whole SCR-relevant temperature range from room temperature to 750 °C. Kinetics for low-temperature reactions are taken from our previous study (Tischer et al., 2019), while high-temperature reactions are developed in the present study. There is still some uncertainty in the second stage of urea decomposition, especially concerning the interplay of the mixture of urea, biuret and triuret. A major issue therefore is the unavailability of thermodynamic data for certain species, in particular for triuret. More experiments, in open and closed vessels, should be done to determine the nature and gather more data of a possible eutectic mixture of biuret and triuret. Nevertheless the mechanism used in this study can reproduce all important processes during decomposition of urea and its by-products. Further investigation of the addressed problems could complete the uncertain parts of the mechanism, make it more robust and enhance its area of application. An implementation of this extended urea decomposition mechanism into CFD simulations of SCR systems could furthermore improve the accuracy of existing models in order to match the experimental deposit composition, help to avoid the formation of high-temperature by-products and make the development process more cost-efficient.

Declaration of Competing Interest

The authors declare that they have no known competing financial interests or personal relationships that could have appeared to influence the work reported in this paper.

Acknowledgements

The authors kindly acknowledge the financial support from the German Research Foundation (Deutsche Forschungsgemeinschaft, DFG) through project 237267381 – TRR 150. DFG is also acknowledged for financing the thermogravimetrical analysis equipment within project INST 121384/70–1. Furthermore, we acknowledge Steinbeis GmbH & Co. KG für Technologietransfer (STZ 240 Reaktive Strömung) for a cost-free license of DETCHEM. We would like to thank the Abgaszentrum Karlsruhe for conducting the experiments.

Appendix A. Supplementary material

Supplementary data associated with this article can be found, in the online version, at https://doi.org/10.1016/j.ces.2021.116876.

References

Bann, B., Miller, S.A., 1958. Melamine And Derivatives Of Melamine. Chem. Rev. 58 (1), 131–172. https://doi.org/10.1021/cr50019a004. ISSN 0009-2665.

Bernhard, A.M., Peitz, D., Elsener, M., Wokaun, A., Kröcher, O., 2012. Hydrolysis and thermolysis of urea and its decomposition byproducts biuret, cyanuric acid and melamine over anatase TiO2. Applied Catalysis B: Environmental 115–116, 129–137. https://doi.org/10.1016/j.apcatb.2011.12.013. ISSN 09263373.

Birkhold, F., 2007. Selektive katalytische Reduktion von Stickoxiden in Kraftfahrzeugen: Untersuchung der Einspritzung von Harnstoffwasserlösung Phd thesis. Karlsruhe Institute of Technology, Karlsruhe, Germany.

M.J. Bojdys, Über neue Allotrope und Nanostrukturen von Karbonitriden: On new allotropes and nanostructures of carbon nitrides, Dissertation, University of Potsdam, Potsdam, http://opus.kobv.de/ubp/volltexte/2010/4123/, 2009.

Börnhorst, M., Deutschmann, O., 2018. Single droplet impingement of urea water solution on a heated substrate. Int. J. Heat Fluid Flow 69, 55–61. https://doi.org/10.1016/j.ijheatfluidflow.2017.10.007. ISSN 0142727X.

Börnhorst, M., Kuntz, C., Tischer, S., Deutschmann, O., 2020. Urea derived deposits in diesel exhaust gas after-treatment: Integration of urea decomposition kinetics into a CFD simulation. Chem. Eng. Sci. 211, 115319. https://doi.org/10.1016/j.ces.2019.115319. ISSN 00092509.

Brack, W., Heine, B., Birkhold, F., Kruse, M., Schoch, G., Tischer, S., Deutschmann, O., 2014. Kinetic modeling of urea decomposition based on systematic thermogravimetric analyses of urea and its most important by-products. Chem. Eng. Sci. 106, 1–8. https://doi.org/10.1016/j.ces.2013.11.013. ISSN 00092509.

Börnhorst, M., Langheck, S., Weickenmeier, H., Dem, C., Suntz, R., Deutschmann, O., 2016. Characterization of solid deposits from urea water solution injected into a hot gas test rig. Chemical Engineering Journal ISSN 13858947. https://doi.org/10.1016/j.cej.2018.09.016.

Brack, W., Heine, B., Birkhold, F., Kruse, M., Deutschmann, O., 2016. Formation of Urea-Based Deposits in an Exhaust System: Numerical Predictions and Experimental Observations on a Hot Gas Test Bench. Emission Control Science and Technology 2 (3), 115–123. https://doi.org/10.1007/s40825-016-0042-2. ISSN 2199-3629.

Budziankou, U., Börnhorst, M., Kuntz, C., Deutschmann, O., Lauer, T., 2020. Deposit Formation from Urea Injection: a Comprehensive Modeling Approach. Emission Control Science and Technology 6 (2), 211–227. https://doi.org/10.1007/s40825-020-00159-x. ISSN 2199-3629.

Crews, G.M., Ripperger, W., Kersebohm, D.B., Güthner, T., Mertschenk, B., 2000. Melamine and Guanamines. In: Ullmann's Encyclopedia of Industrial Chemistry. Wiley-VCH Verlag GmbH & Co. KGaA, Weinheim, Germany. https://doi.org/10.1002/14356007.a16_171.pub2. ISBN 3527306730.

O. Deutschmann, S. Tischer, S. Kleditzsch, V. Janardhanan, C. Correa, D. Chatterjee, N. Mladenov, H.D. Minh, H. Karadeniz, M. Hettel, V. Menon, A. Banerjee, 2018. DETCHEM Software package, ed. 2.7, URL www.detchem.com.

Ebrahimian, V., Nicolle, A., Habchi, C., 2012. Detailed modeling of the evaporation and thermal decomposition of urea-water solution in SCR systems. AIChE J. 58 (7), 1998–2009. https://doi.org/10.1002/aic.12736. ISSN 00011541.

Eichelbaum, M., Farrauto, R.J., Castaldi, M.J., 2010. The impact of urea on the performance of metal exchanged zeolites for the selective catalytic reduction of NOxPart I. Pyrolysis and hydrolysis of urea over zeolite catalysts. Applied Catalysis B: Environmental 97 (1–2), 90–97. https://doi.org/10.1016/j.apcatb.2010.03.027. ISSN 09263373.

Fang, H.L., DaCosta, H.F., 2003. Urea thermolysis and NOx reduction with and without SCR catalysts. Applied Catalysis B: Environmental 46 (1), 17–34. https://doi.org/10.1016/S0926-3373(03)00177-2. ISSN 09263373.

Gratzfeld, D., Olzmann, M., 2017. Gas-phase standard enthalpies of formation of urea-derived compounds: A quantum-chemical study. Chem. Phys. Lett. 679, 219–224. https://doi.org/10.1016/j.cplett.2017.05.006. ISSN 00092614.

Güthner, T., Mertschenk, B., 2000. Cyanamides. In: Ullmann's Encyclopedia of Industrial Chemistry. Wiley-VCH Verlag GmbH & Co. KGaA, Weinheim, Germany. https://doi.org/10.1002/14356007.a08_139.pub2. ISBN 3527306730.

Gross, P., Höppe, H.A., 2020. Biuret, a Crucial Reaction Intermediate for Understanding the Urea Pyrolysis to Carbon Nitrides: Crystal Structure Elucidation and In Situ Diffractometric, Vibrational and Thermal Characterisation. Chemistry (Weinheim an der Bergstrasse, Germany). https://doi.org/10.1002/chem.202001396.

Hirshfeld, F.L., Hope, H., 1980. An X-ray determination of the charge deformation density in 2-cyanoguanidine. Acta Crystallographica Section B Structural Crystallography and Crystal Chemistry 36 (2), 406–415. https://doi.org/10.1107/S0567740880003366. ISSN 0567-7408.

Jürgens, B., Irran, E., Senker, J., Kroll, P., Müller, H., Schnick, W., 2003. Melem (2,5,8-triamino-tri-s-triazine), an important intermediate during condensation of melamine rings to graphitic carbon nitride: synthesis, structure determination by X-ray powder diffractometry, solid-state NMR, and theoretical studies. J. Am. Chem. Soc. 125 (34), 10288–10300. https://doi.org/10.1021/ja0357689. ISSN 0002-7863.

Krum, K., Patil, R., Christensen, H., Hashemi, H., Wang, Z., Li, S., Glarborg, P., Wu, H., 2021. Kinetic modeling of urea decomposition and byproduct formation. Chem. Eng. Sci. 230, 116138. https://doi.org/10.1016/j.ces.2020.116138. ISSN 00092509.

Liebig, J., 1834. Ueber einige Stickstoff - Verbindungen. Annalen der Pharmacie 10 (1), 1–47. https://doi.org/10.1002/jlac.18340100102. ISSN 03655490.

Liu, A.Y., Cohen, M.L., 1989. Prediction of new low compressibility solids. Science (New York, N.Y.) 245 (4920), 841–842. https://doi.org/10.1126/science.245.4920.841. ISSN 0036-8075.

Lotsch, B.V., 2006. From molecular building blocks to condensed carbon nitride networks, Dissertation. Ludwig Maximilans Universität, München.

Lotsch, B.V., Schnick, W., 2005. Thermal Conversion of Guanylurea Dicyanamide into Graphitic Carbon Nitride via Prototype CN x Precursors. Chem. Mater. 17 (15), 3976–3982. https://doi.org/10.1021/cm050350q. ISSN 0897-4756.

Lotsch, B.V., Schnick, W., 2007. New light on an old story: formation of melam during thermal condensation of melamine. Chemistry (Weinheim an der Bergstrasse, Germany) 13 (17), 4956–4968. https://doi.org/10.1002/chem.200601291.

Lundström, A., Andersson, B., Olsson, L., 2009. Urea thermolysis studied under flow reactor conditions using DSC and FT-IR. Chem. Eng. J. 150 (2–3), 544–550. https://doi.org/10.1016/j.cej.2009.03.044. ISSN 13858947.

Lundström, A., Snelling, T., Morsing, P., Gabrielsson, P., Senar, E., Olsson, L., 2011. Urea decomposition and HNCO hydrolysis studied over titanium dioxide. Fe-Beta and gamma-Alumina, Applied Catalysis B: Environmental 106 (3–4), 273–279. https://doi.org/10.1016/j.apcatb.2011.05.010. ISSN 09263373.

May, H., 1959. Pyrolysis of melamine. J. Appl. Chem. 9 (6), 340–344. https://doi.org/10.1002/jctb.5010090608. ISSN 00218871.

Mccellan, P.P., 1940. Melamine Preparation. Industrial & Engineering Chemistry 32 (9), 1181–1186. https://doi.org/10.1021/ie50369a026. ISSN 0019-7866.

Michaud, H., Goll, W., Hammer, B., von Seyerl, J., Sturm, W., Weiss, S., Youngman, R., 1988. Die Bildung von Harnstoffen aus Cynamiden: Wissenschaftlich und technisch beachtenswerte Reaktionen und deren praktische Bedeutung. Chemiker Zeitung 112 (10), 287–294.

Miller, T.S., Jorge, A.B., Suter, T.M., Sella, A., Corà, F., McMillan, P.F., 2017. Carbon nitrides: synthesis and characterization of a new class of functional materials. Physical chemistry chemical physics: PCCP 19 (24), 15613–15638. https://doi.org/10.1039/C7CP02711G.

Ostrogovich, G., Bacaloglu, R., 1965. Die Kinetik der Thermolyse von Harnstoff und der darauffolgenden Umwandlungen. II, Revue Roumaine de Chimie 10, 1111–1128.

Postrioti, L., Brizi, G., Ungaro, C., Mosser, M., Bianconi, F., 2015. A methodology to investigate the behaviour of urea-water sprays in high temperature air flow for SCR de- NOx applications. Fuel 150, 548–557. https://doi.org/10.1016/j.fuel.2015.02.067. ISSN 00162361.

C. Habchi, A. Nicolle, N. Gillet, Numerical study of Urea-Water Solution injection and deposits formation in an SCR System, doi:10.13140/RG.2.1.3171.2481, 2015.

M. Quissek, T. Lauer, O. García-Afonso, S. Fowles, Identification of Film Breakup for a Liquid Urea-Water-Solution and Application to CFD, in: SAE Technical Paper Series, SAE Technical Paper Series, SAE International400 Commonwealth Drive, Warrendale, PA, United States, 2019, doi:10.4271/2019-01-0983.

Ruan, L., Xu, G., Gu, L., Li, C., Zhu, Y., Lu, Y., 2015. The physical properties of Li-doped g-C3N4 monolayer sheet investigated by the first-principles. Mater. Res. Bull. 66, 156–162. https://doi.org/10.1016/j.materresbull.2015.02.044. ISSN 00255408.

Salley, D.J., Gray, J.B., 1948. Heats of Combustion of Some Organic Nitrogen Compounds. J. Am. Chem. Soc. 70 (8), 2650–2653. https://doi.org/10.1021/ja01188a011. ISSN 0002-7863.

Schaber, P.M., Colson, J., Higgins, S., Thielen, D., Anspach, B., Brauer, J., 2004. Thermal decomposition (pyrolysis) of urea in an open reaction vessel. Thermochim. Acta 424 (1–2), 131–142. https://doi.org/10.1016/j.tca.2004.05.018. ISSN 00406031.

Selivanov, V., Karlik, V.M., Zagranicnyi, V.I., 1973. Standard enthalpies of formation ammeline, ammelide, melem, and melon. Russ. J. Phys. Chem 47.

Smolin, E.M., Rapoport, L. (Eds.), 1959. Chem. Heterocycl. Compd.. Chemistry of Heterocyclic Compounds: A Series Of Monographs. John Wiley & Sons, Inc, Hoboken, NJ, USA. ISBN 9780470186626, doi:10.1002/9780470186626.

Stradella, L., Argentero, M., 1993. A study of the thermal decomposition of urea, of related compounds and thiourea using DSC and TG-EGA. Thermochim. Acta 219, 315–323. https://doi.org/10.1016/0040-6031(93)80508-8. ISSN 00406031.

Y. Sun, S. Sharma, B. Vernham, K. Shibata, S. Drennan, Urea Deposit Predictions on a Practical Mid/Heavy Duty Vehicle After-Treatment System, in: SAE Technical Paper Series, SAE Technical Paper Series, SAE International400 Commonwealth Drive, Warrendale, PA, United States, 2018, doi:10.4271/2018-01-0960.

Tischer, S., Börnhorst, M., Amsler, J., Schoch, G., Deutschmann, O., 2019. Thermodynamics and reaction mechanism of urea decomposition. Physical chemistry chemical physics: PCCP 21 (30), 16785–16797. https://doi.org/10.1039/c9cp01529a.

Wang, D., Dong, N., Niu, Y., Hui, S., 2019. A Review of Urea Pyrolysis to Produce NH 3 Used for NO x Removal. Journal of Chemistry 2019, 1–11. https://doi.org/10.1155/2019/6853638. ISSN 2090-9063.

Wirnhier, E., Mesch, M.B., Senker, J., Schnick, W., 2013. Formation and characterization of melam, melam hydrate, and a melam-melem adduct. Chemistry (Weinheim an der Bergstrasse, Germany) 19 (6), 2041–2049. https://doi.org/10.1002/chem.201203340.

Yin, L.-W., Li, M.-S., Liu, Y.-X., Sui, J.-L., Wang, J.-M., 2003. Synthesis of beta carbon nitride nanosized crystal through mechanochemical reaction. J. Phys.: Condens. Matter 15 (2), 309–314. https://doi.org/10.1088/0953-8984/15/2/330. ISSN 0953-8984.

Yin, L.-W., Bando, Y., Li, M.-S., Liu, Y.-X., Qi, Y.-X., 2003. Unique Single-Crystalline Beta Carbon Nitride Nanorods. Adv. Mater. 15 (21), 1840–1844. https://doi.org/10.1002/adma.200305307. ISSN 0935-9648.

Zhang, J.-B., Tan, Z.-C., Meng, S.-H., Li, S.-H., Zhang, L.-M., 1997. Heat capacity and thermal decomposition of dicyandiamide. Thermochim. Acta 307 (1), 11–15. https://doi.org/10.1016/S0040-6031(97)00323-7. ISSN 00406031.

Zhang, X., Qian, G., Yang, X., Hu, C., Zhou, X., 2014. Solid–liquid equilibrium of dicyandiamide in different solvents. Fluid Phase Equilib. 363, 228–232. https://doi.org/10.1016/j.fluid.2013.12.001. ISSN 03783812.

Zhu, J., Wei, Y., Chen, W., Zhao, Z., Thomas, A., 2010. Graphitic carbon nitride as a metal-free catalyst for NO decomposition. Chemical communications (Cambridge, England) 46 (37), 6965–6967. https://doi.org/10.1039/c0cc01432j.

Zhu, J., Xiao, P., Li, H., Carabineiro, S.A.C., 2014. Graphitic carbon nitride: synthesis, properties, and applications in catalysis. ACS applied materials & interfaces 6 (19), 16449–16465. https://doi.org/10.1021/am502925j.

Burcat A., 2006. Burcat's Thermodynamic Data, URL http://garfield.chem.elte.hu/Burcat/burcat.html.